Proceedings of the 25th International Conference on
**Port and Ocean Engineering under Arctic Conditions**
June 9-13, 2019, Delft, The Netherlands

# A study of drag force on an ice ridge keel in stratified fluids

Yongheng Zu[1], Peng Lu[2], Zhijun Li[2], Yuanren Xiu[2], Miao Yu[2], Xiaowei Cao[2]
[1] Affiliation of first author(s) (Dalian university of technology, Dalian, China)
[2] Affiliation of co-author(s) (Dalian university of technology, Dalian, China)

## ABSTRACT

The halocline of Arctic ocean tends to be shallow in summer and internal waves by the draft of ice ridge keels will be generated at the interface of stratified fluids. Internal waves have an important impact on the drag force of an individual ridge keel with various flow velocities, keel depths and slope angles. In this study, the physical and numerical simulation are performed to investigate the influence of various keel topography on an individual ridge keel drag coefficient in stratified fluids. Variations of drag forces and drag coefficient are obtained, and the numerical simulation results agree well with the physical results. When $Fr<1$, the drag coefficient increases first and then decreases with increasing $Fr$. When $Fr>1$, the drag coefficient tends to be stable. The drag coefficient varies linearly with the depth of the ice ridge keel into the water and has nonlinear relationship of the slope angle of the ice ridge keel.

KEY WORDS: Ice ridge; Drag coefficient; Internal wave; Froude number.

## INTRODUCTION

The Arctic resource development and shipping navigation have gradually been important research topics, because the Arctic sea ice extent has continued to shrink in recent years (Snape, et al., 2014; Han, et al., 2015). The ice-related structures are mostly located in the marginal ice zone, and higher requirements are needed to solve problems of sea ice dynamics in these areas. The sea ice in the marginal zone is strongly exchanged by the effects of solar radiation, wind, waves, and currents. The balance of both energy and momentum between the atmosphere and the ocean forms a closely coupled system (Morison, et al., 1987). The sea ice drag coefficient is a parameter describing the exchange efficiency of momentum of sea ice with the atmosphere and ocean, and is also a necessary input for the numerical modeling of sea ice dynamics (Lu, et al., 2011). The traditional methods for determining the drag coefficient of sea ice mainly include eddy method (Fujisaki, et al., 2009), profile method (Andreas, et al., 1995), and momentum method (Pease, et al., 1983). These methods are applicable to specific sea areas and sea ice types, neglecting the influence of the shape and boundary conditions of sea ice itself on

the dynamic process of sea ice, so that some discrete results are obtained by these methods.

The parameterization of the sea ice drag coefficient aims to establish a quantitative relationship between the factors and drag coefficient, including sea ice concentration, surface roughness, size, surface melt ponds distribution and other related parameters. The sea ice drag coefficient, changing with the sea ice condition, also makes the model result closer to the actual situation (Lu, et al. 2011; Tsamados, et al., 2014; Luepkes, et al., 2012). According to the parametric idea, the sea ice drag coefficient consists of two parts: the skin drag coefficient and the form drag coefficient. The skin drag coefficient describes the shear force caused by the distribution of small roughness on uniform sea ice surface. The form drag coefficient describes horizontal pressure difference in the flow field caused by changes in the boundary of sea ice and large protrusions such as ice ridge (Andreas, 1995), and different types of surface roughness are divided by the cut height (Tan, et al., 2012). The contribution of the form drag force to the total drag coefficient can be defined by the following formula:

$$C_w^r = \frac{C_r A h_r}{\pi D_r}\left[1 - \left(\frac{h_r}{D_r}\right)^{1/2}\right]^2 \quad (1)$$

where $A$ is the sea ice concentration, $h_r/D_r$ is the ice ridge intensity, the ratio of the draught water depth of the ice ridge to the distance between ridges, and $C_r$ is the local drag coefficient of a single ice ridge. When the ice ridge is large, the contribution of the ice ridge drag force is not negligible (Lu, et al., 2011).If $A$ and $h_r/D_r$ are certain, the local drag coefficient $C_r$ of a single ice ridge directly determines the form drag coefficient. Therefore, studying the local drag coefficient of a single ice ridge is of great significance for the study of momentum exchange at the ice-water interface.

Some studies have been conducted about local drag coefficient that generally considers the movement of ice ridge in a uniform fluid. However, in recent years, the rapid melting of the Arctic summer sea ice results in halocline to become shallower. And it has been observed that the halocline depth is in the same order of magnitude of the ice ridge depth in the marginal zone of sea ice, which has a significant influence on the ice ridge drag force (Randelhoff, et al., 2014; McPhee, 2012; Lu, et al., 2016). The two-layer fluid can simply simulate stratification, and the operability of the physical experiment is also possible. Although the two-layer flow environment is only a simple simulation of the stratification of the Arctic ocean, it can reflect the dynamic characteristics of different flow conditions. Pite (1995) carried out a physical experiment on this problem, combined with Baines' (1984) description of the state of the internal wave, the experimental groups cover transcritical region, subcritical region, and supercritical region. During the operation of the ice ridge in the transcritical region, obvious internal wave resistance is encountered. The disturbance generated under the ice ridge propagates upstream, forming a nonlinear internal wave downstream of the ice ridge with the resonance energy propagation, White (2012) improved Baines' method and studied the problem of energy propagation. Grue (2015) used the boundary element theory to develop a nonlinear method for calculating the two-layer flow and compared results with the method for solving the Korteweg-de Vries (KdV) equation. The numerical simulation of this problem has always been a research focus. Jammel (1993) used finite difference algorithm based on the Euler equation to numerically simulate the stratified fluid and compared results with the physical experiment conducted by Pite; Mortikov (2016) adopted the immersion boundary method to treat the boundary of fluid. Most of these previous studies have qualitatively analyzed the internal wave and the drag forces generated by the internal wave, and did not establish the parameterized relationship between the ice ridge morphology and the ice-water drag coefficient in the two-layer flow.

With the development of computational fluid dynamics in recent years, the computational efficiency of turbulence models has been greatly improved by implementing parallel computation. In this paper, the RNG k-ε turbulence model and the interface tracking method of VOF are used to numerically simulate this problem. The flow field data in the numerical

simulation is post-processed, and the effect of dynamic pressure on the internal wave resistance is analyzed in comparison with the results of the physical experiment. The variation law of local drag coefficients of the ice ridge is given along with the draught water depth of the ice ridge and the Froude number.

## EXPERIMENTS

The physical experiments were completed at the Particle Image Velocimetry (PIV) tank in the State Key Laboratory of Coastal and Offshore Engineering (SLCOE) in Dalian University of Technology (see Figure 1). The tank is 450 cm long, 23 cm wide and 45 cm deep. Pipes are laid at the bottom of the tank. Fresh water is added to the tank and then brine is added to form the upper and lower layers. The upper layer is 15 cm deep and the lower layer is 20 cm deep. The material of the ice ridge model is plexiglass, and the base angle of the ice ridge is designed to be 45 °(see Figure 1). The ice ridge model is run on the track along the free surface under the rotation of the motor, and the towing speeds of ice ridge can be set to constant motion ranging from 1 cm/s to 30 cm/s. The depth of the ice ridge into the water is also adjustable and the range is from 4 cm to 10 cm. The ice ridge model is connected to the tension pressure sensor to measure the drag force due to the motion of the ice ridge in two-layer fluids. The relevant parameters is listed in Table 1.

Table 1. Parameters used in physical experiment with a two-layer fluid

| Parameters | | Symbols | Values | Units |
|---|---|---|---|---|
| tank | dimensions | $L\times W\times H$ | 450×23×45 | cm |
| | slope angle | $\theta$ | 45 | ° |
| ice ridge | keel depth | $h$ | 4-10 | cm |
| | towing speed | $U$ | 1-30 | cm/s |
| fluid 1 | depth | $h_1$ | 15 | cm |
| | density | $\rho_1$ | 998.2 | kg/m3 |
| | viscosity coefficient | $\mu_1$ | $1.0003\times10^{-3}$ | kg/(m·s) |
| fluid 2 | depth | $h_2$ | 20 | cm |
| | density | $\rho_2$ | 1025 | kg/m3 |
| | viscosity coefficient | $\mu_2$ | $1.12\times10^{-3}$ | kg/(m·s) |
| | maximum phase speed | $\varphi$ | 14 | cm/s |
| | Froude number | $Fr$ | 0.07-2.14 | |

The experiments simulate the generation of internal wave and follow the principle of Froude number similarity. In the two-layer fluids, The ratio of the amplitude of the internal wave to the surface wave is equal to $(\rho_1-\rho_a)/(\rho_2-\rho_1)\approx37$, so the influence of surface wave is negligible (Mercier, et al., 2011). Thus, the experimental state and the actual state should satisfy equal Froude number. The Froude number is a dimensionless parameter that reflects the ratio of gravity to inertial force, defined here as the ratio of the towing speed of ice ridge to the speed of the linear internal wave phase speed.

$$Fr = \frac{U}{\varphi} \tag{2}$$

where $U$ is the towing speed of ice ridge, $\varphi$ is the linear internal wave phase speed. Here the internal wave phase speed uses a linear non-dispersion long-wave phase speed (Melville, et al., 1987).

$$\varphi^2 = \sigma g h_0,\ \sigma = \frac{\rho_2 - \rho_1}{\rho_0},\ h_0 = \frac{h_1 h_2}{h_1 + h_2} \tag{3}$$

where $\rho_0$ and $h_0$ are the characteristic density and depth in the model, and the internal wave phase speed in this experiment is about 14 cm/s. Pite (1995) investigated some field observation data show that when the ice ridge drift speed is about 0.2 m/s and the keel depth is about 10 m, the range of Froude number is 0.12~0.69, and the range of the ratio of the keel depth into the water to the depth of the upper fluid is 0.12~1.38, but in later observation data, The range of Froude number can reach 0.2~3.8 (Pite, et al., 1995; Amundrud, et al., 2006). In numerical simulation and physical simulation experiments, the range of Froude number is 0.07~2.14, and the range of the ratio of the depth of ice ridge into water to upper fluid depth is 0.27~0.67, which ensures that the experimental results can cover different internal wave forms in the field, including subcritical, transcritical and supercritical region.

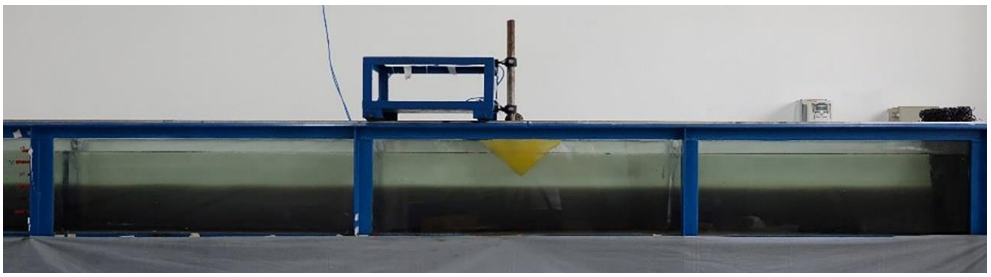

Figure 1. Physical setup of an ice ridge keel dragged by a motor with constant speed

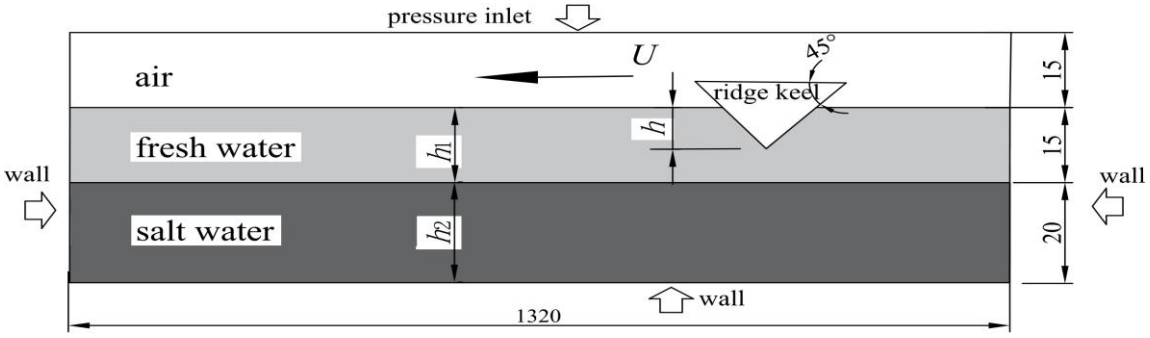


Figure 2. Sketch of numerical tank

Considering that the fluid speed remains constant over the width of the tank, the numerical simulation is simplified into a two-dimensional problem. The setting of the numerical experiments is identical to the simulations from a physical model of the previous stage in the vertical dimension. The computational domain of the numerical tank is doubled in length due to the influence of the side boundaries for a total length of 1320 cm. Fluid property parameters in numerical experiments are consistent with physical experiments. The initial speed of the fluid is 0, which is consistent with the experimental group of the physical model test, as shown in Figure 2. The computational domain contains triangular grids and quadrilateral grids. The type of grids near the ice ridge is unstructured, and the type of other grids is structured. At the same time, The upper part containing the ice ridge portion is set as dynamic mesh, the ice ridge boundary moves toward the left at a constant towing speed, and the lower part is stationary mesh; The boundary between the dynamic mesh and the static mesh is a pair of internal interfaces.

The control equation calculated by the flow field is the k-ε turbulence model based on the Reynolds stress average equation. For the RNG *k-ε* model, the two equations are as follows:

$$\frac{\partial}{\partial t}(\rho k) + \frac{\partial}{\partial x_i}(\rho k U_i) = \frac{\partial}{\partial x_i}\left(\alpha_k \mu_{eff} \frac{\partial k}{\partial x_i}\right) + G_k + G_b - \rho\varepsilon - Y_M + S_k \tag{4}$$

$$\frac{\partial}{\partial t}(\rho \varepsilon) + \frac{\partial}{\partial x_i}(\rho \varepsilon U_i) = \frac{\partial}{\partial x_i}\left(\alpha_\varepsilon \mu_{eff} \frac{\partial \varepsilon}{\partial x_i}\right) + C_{1\varepsilon}\frac{\varepsilon}{k}(G_k + C_{3\varepsilon}G_b) - C_{2\varepsilon}\rho\frac{\varepsilon^2}{k} - R_\varepsilon + S_\varepsilon \tag{5}$$

where $C_\mu$=0.0845, $C_{1\varepsilon}$=1.42, $C_{2\varepsilon}$=1.68, $\alpha_\varepsilon$=$\alpha_k$=1.39. The control equation of numerical

simulation adopts first-order implicit integration in the temporal discretization, and the second-order upwind scheme is adopted in the spatial discretization. The Pressure-Implicit with Splitting of Operators (PISO) pressure-velocity coupling scheme, part of the SIMPLE family of algorithms, is a typical multi-step correction time splitting algorithm. Because this model is multi-phase flow and the solver need to calculate transient flow field information, the PISO scheme is adopted. The motion of ice ridge adopts dynamic mesh module, which is solved by using the layering scheme. The Volume of fluid (VOF) model is applied for the tracking of the interface of two-layer fluids, and the interpolation near the interface selects geometric reconstruction approach. This is also a more accurate interface tracking method at present, which is recommended by most transient VOF calculations.

## RESULTS

For the convenience of the analysis, a dimensionless parameter related to the internal wave is introduced. The dimensionless depth $B$ is defined as the ratio of the keel depth into water $h$ to the upper fluid depth $h_1$.

$$B = \frac{h}{h_1} \tag{6}$$

The local drag coefficient $C_r$ of a single ice ridge uses the form of the drag coefficient:

$$C_r = \frac{F}{\rho_1 A U^2} \tag{7}$$

where $F$ is the drag force of a single ice ridge, $\rho_1$ is the density of upper fluid, $A$ is the projected area of a single ice ridge in the direction perpendicular to the free surface, $U$ is the towing speed of the ice ridge.

### Variations with Froude number

Drag force of a single ice ridge in the numerical simulation is obtained from the integration of the pressure stress and the vicious stress along ice ridge boundary lines. The force results of the numerical simulation match well with the physical results, see Figure 3. When the Froude number Fr<1, the relationship between drag force and Froude number shows nonlinearity. Drag force increases first and then decreases with increasing Fr. When Fr>1, the variation of drag force become monotonously increased with the growth of Fr. Nonlinearity is more evident in the variation law of the drag coefficient which tends to 1 with Fr>1. The drag coefficient of uniform fluid is stable at around 1. The accuracy of force sensor in physical model experiment, less than 0.001N, is relatively lower than that in numerical condition, that accounts for some unsatisfactory results at smaller Fr.

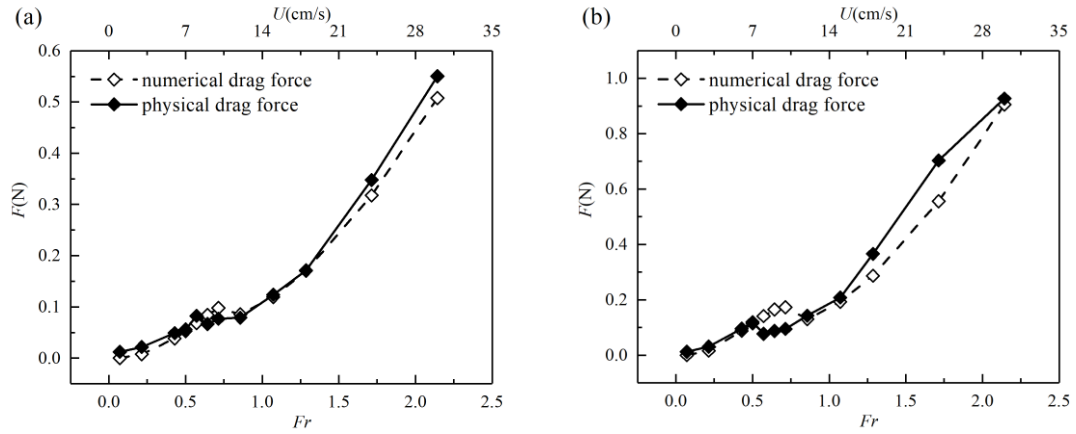

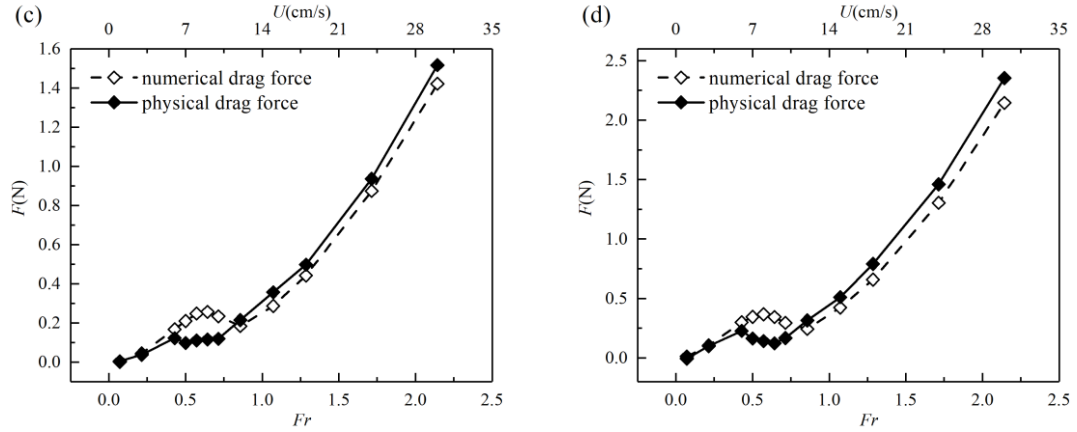


Figure 3. Variations of drag force with Froude number, (a) when keel depth $h$=4 cm, (b) $h$=6 cm, (c) $h$=8 cm, (d) $h$=10 cm. The dashed line marks numerical result, the soli d line marks physical result.

The numerical results give smaller values of drag force than physical results in the nonlinear region due to the fact that interfaces of two layer fluids have some difference between numerical and physical condition. The interface in numerical simulation is a sharp pycnocline rather than a continuous pycnocline between two layers in physical condition, see Figure 4, plotting different density profiles and buoyancy frequency profiles in two experiments. Buoyancy frequency $N$ is defined as follow:

$$N = \sqrt{\frac{g}{\bar{\rho}}\frac{d\bar{\rho}}{dz}} \tag{8}$$

There is a transition region of about 7 cm height at interface in physical model, where N≈3rad/s. For the absolutely continuous stratified fluids, the internal wave phase speed c with h =35cm is computed as follow:

$$C = \frac{N(h_1+h_2)}{\pi} = 8.1\text{cm/s} \tag{9}$$

For the simple condition of two layer fluids, the internal wave phase speed with $h_1$=15 cm, $h_2$=20 cm is computed as follow:

$$C = \sqrt{(\frac{g}{\rho_0}\frac{\rho_2-\rho_1}{h_2+h_1}h_1h_2)} = 14.4\text{cm/s} \tag{10}$$

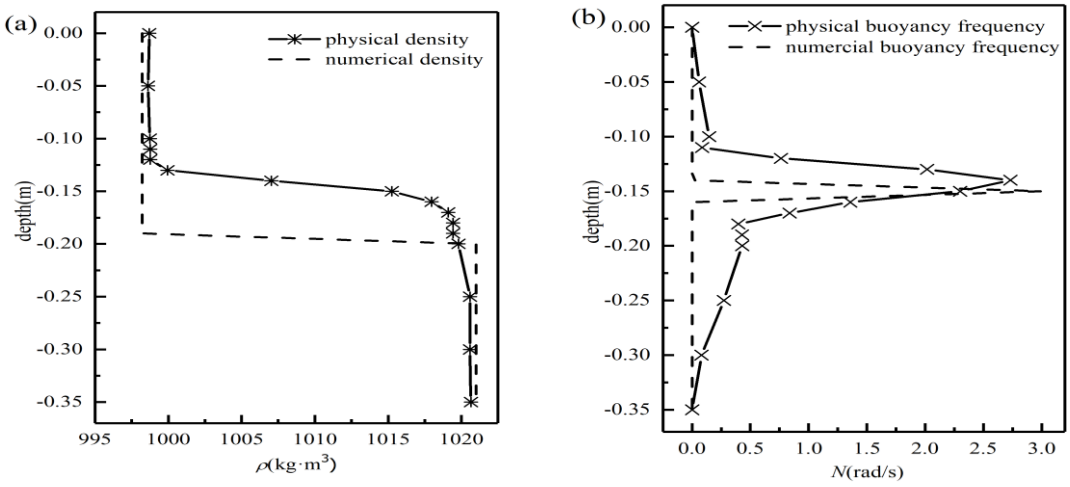


Figure 4. (a) Comparison of vertical density profile in numerical (dash line) and physi cal simulation (solid line), (b) Comparison of vertical buoyancy frequency profile in n umerical (dash line) and physical simulation (solid line).

The phase speed $C$ is positively correlated with the density gradient. The density gradient of numerical simulation at the interface is larger than physical experiment. For physical tank, it is

a continuous layer in the vicinity of the interface, and belongs to the two-layer flow case as a whole. The actual internal wave phase speed should be less than the numerical condition, in the range between 8.1 cm/s and 14.4 cm/s, and close to 14.4 cm/s, accounting for a certain difference between the numerical and the physical results. The numerical model is more ideal than the physical model.

When $Fr > 1$, internal waves have little effect on drag force, and the variation of the drag force with $Fr$ is similar to that of the uniform fluid. At this region, numerical and physical results agree well. Figure 5 shows numerical drag force compared between the stratified flow and the uniform flow with the draught depth of the ice ridge $h = 8$ cm. It can be seen from the Figure 5 that the resistance results of the two layer flow is more complicated than the single layer flow. With $Fr = 1$ as the critical point, the resistance difference in the front section is large, due to the generation of internal waves, which has a great influence on the pressure field behind the ice ridge. It will be analyzed in detail later in this paper. When $Fr > 1$, the influence of internal wave on the resistance of ice ridge is almost negligible. The drag coefficients of the ice ridge of two layer and uniform flow approach a constant, as shown in Figure 5. The specific value is also affected by the draught depth of the ice ridge.

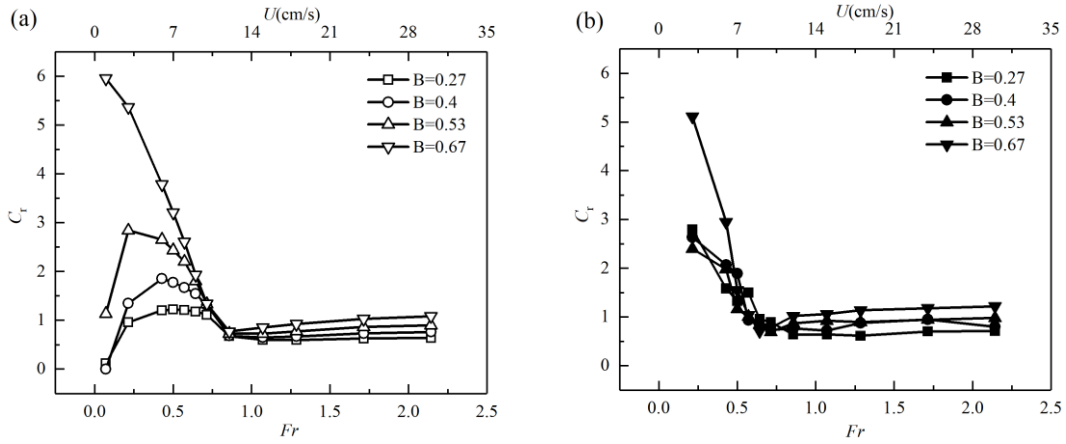


Figure 5. Variations of drag coefficient with Froude number of different keel depths $B$ =0.27, $h$ = 4 cm (inverse triangles); $B$ = 0.4, $h$ = 6 cm (triangles); $B$ = 0.53, $h$ = 8 cm (c ircles); $B$ = 0.67, $h$ = 10 cm (squares), (a) in numerical simulation, (b) in physical sim ulation.

## Variations with keel depth

Figure 6 illustrates the variation the drag coefficient of the ice ridge in the stratified flow with the dimensionless keel depth $B$ with $Fr$ = constant, the drag coefficient is proportional to the keel depth of the ice ridge, which is close to a linear change. When $Fr > 0.57$, the gradient of the drag coefficient with dimensionless depth is relatively small and the value of coefficients approach 1, as shown in Figure 6 with $Fr = 0.86$, $Fr = 1.07$ and $Fr = 2.14$; The gradient of drag coefficient tend to larger with smaller $Fr$.

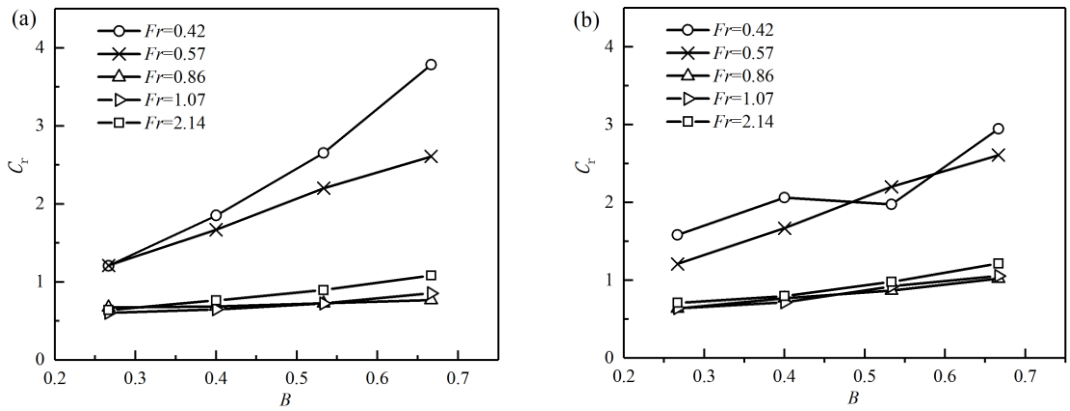


Figure 6. Drag coefficient as a function of keel depth with $Fr$ = 0.42, $U$ = 6 cm/s (circles); $Fr$ = 0.57, $U$ = 8 cm/s (forks); $Fr$ = 0.86, $U$ = 12 cm/s (triangles); $Fr$ = 1.07, $U$ = 15 cm/s (left triangles); $Fr$ = 2.14, $U$ = 30 cm/s (squares), (a) in numerical simulation, (b) in physical simulation.

**Internal wave**

Internal waves generate in the wake of the motion of the ice ridge with different shapes. When the flow condition belongs to nonlinear region, in which the drag coefficient varies with the Froude number, the internal wave speed is greater than the drag speed of the ice ridge accounting for a phenomenon that the internal wave disturbance can propagate simultaneously upstream and downstream. Meanwhile, the internal wave propagates to a certain distance downstream and disappears. The internal wave shape is as shown in Figure 7, and it can be seen that the depression, liking an approximately gentle line, at the interface under the ice ridge extends upstream, and the amplitude of the fluctuation is very small. The internal wave formed downstream is relatively stable, and the position of the peak relative to the ice ridge remains unchanged.

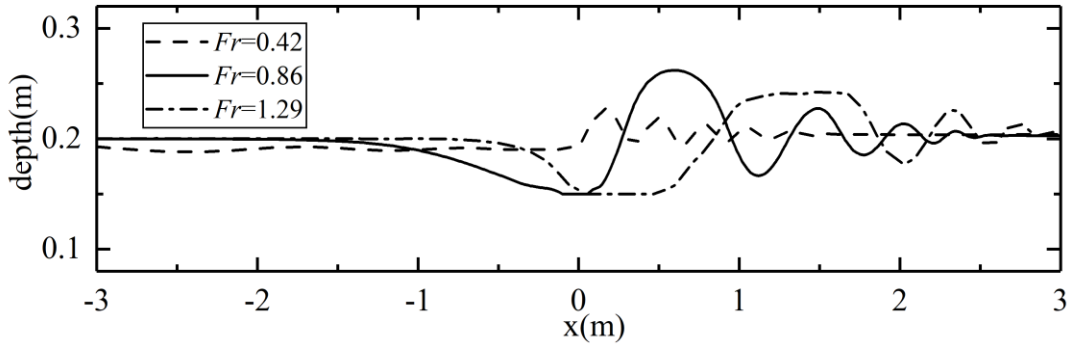


Figure 7. Shapes of internal wave in numerical simulation with $Fr$ = 0.42, $U$ = 6 cm/s (dashed line); $Fr$ = 0.86, $U$ = 12 cm/s (solid line); $Fr$ = 1.29, $U$ = 18 cm/s(dot dash line), when keel depth $h$ = 6 cm. The position of the ice ridge keel is located at x = 0.

As $Fr$ increases, the disturbance along upstream disappears, and the depression only occurs below the ice ridge. At same time, the internal wave downstream is still in a relatively stable state. When $Fr$ > 1, since the drag speed of the ice ridge exceeds the phase speed of the internal wave, the disturbance is no longer fixed to the position around the ice ridge, and propagates downstream in the form of fluctuation with the first peak of internal waves gradually moving away from the ice ridge. When $Fr$ = 2.1, the internal wave shape becomes more messy, the fluctuation keep away from the ice ridge, and finally the disturbance gradually disappears. The fluid state transitions to the supercritical region. The shapes of the internal wave generated under other conditions is similar to that with keel depth $h$ = 6cm, except for that the height of the peak is different. The wave height of numerical simulation is larger than that of physical simulation, because the mixing phenomenon in the physical tank is more obvious, thus

consuming more energy, see Figure 8. Therefore, the wave shape in the numerical tank is relatively stable, and the wave height is higher than that of the physical tank.

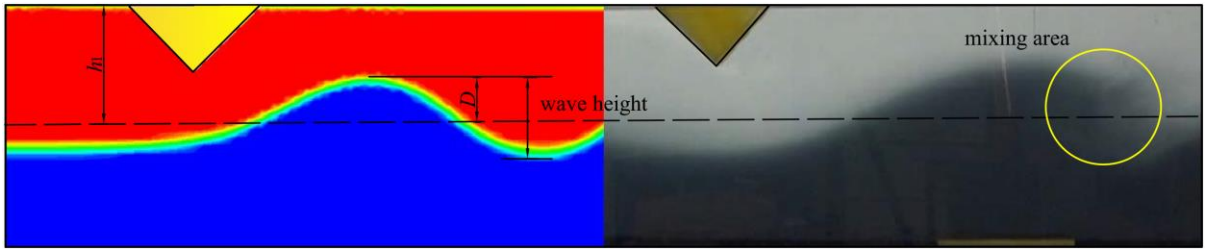


Figure 8. The first internal wave peak around the ridge keel (yellow inverse triangle) in numerical tank (left plotted) and physical tank (right plotted). The mixing phenomenon in the physical tank is more obvious.

## DISCUSSIONS

It has been obvious that the internal wave has an important influence on the drag force of the ice ridge in the nonlinear region. In response to this problem, the two aspects, perpendicular to the running direction of the ice ridge and parallel to that direction, is analyzed about the influence of internal wave changes on the drag force.

Firstly, for the vertical direction, the statistics of maximum interface displacement $D$ of the nonlinear region is calculated. The variation of the displacement with Fr is shown in Figure 9 and the interface displacement $D$ from the initial interface to the peak point is illustrated in Figure 8.

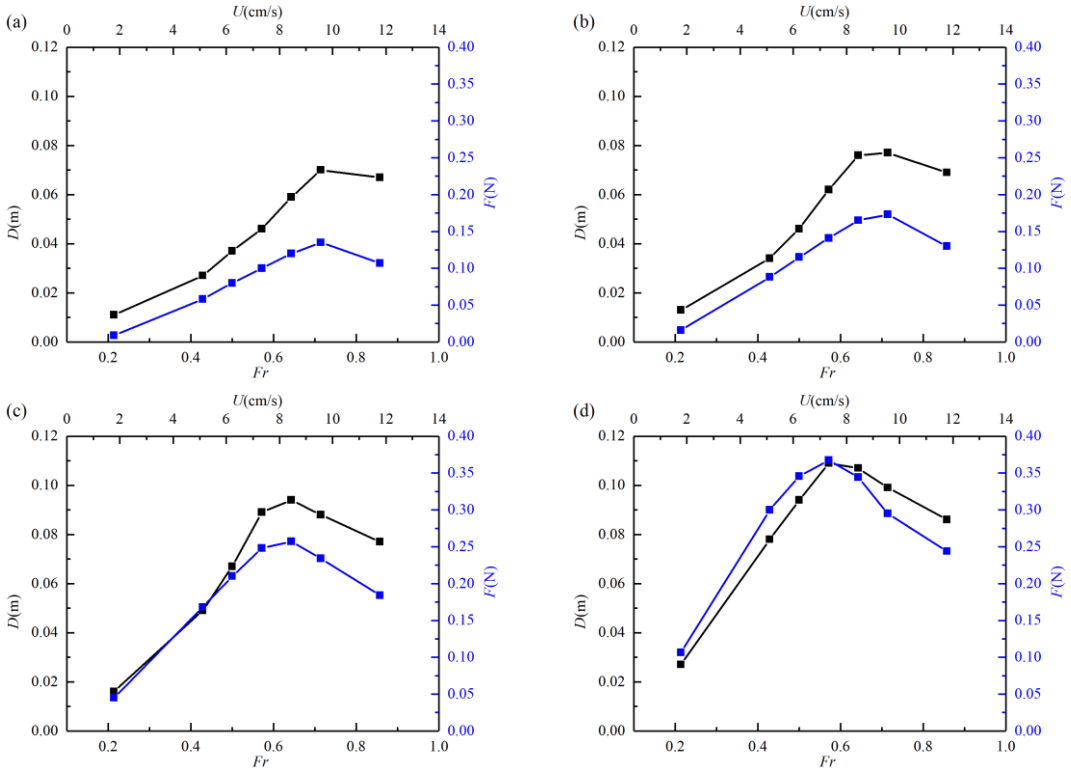


Figure 9. Correlation analysis of interface displacement (black) and drag force (blue) with Froude number, (a) when keel depth $h$ = 4 cm, (b) $h$ = 6 cm, (c) $h$ = 8 cm, (d) $h$ = 10 cm.

The interface displacement $D$ and the drag force $F$ are highly correlated in the transcritical region, and the correlation coefficient $R^2$ of $D$ and $F$ is more than 0.94. The change in the displacement of the interface can reflect the change of the potential energy of the fluid, and at the same time, the speed will increase due to the narrow beam of the upper layer flow. The

potential energy and the kinetic energy of the upper stream is increased at this peak, and the lower layer fluid acts negatively on the upper fluid by shear stress, and the pressure of the streamline is reduced. Finally, a relatively lower pressure zone is formed at the peak of the interface.

In addition, for the horizontal direction, the drag force of the ice ridge is mainly caused by the change of the pressure difference around the ice ridge. Therefore, the dynamic pressure field near the ice ridge which is obtained by subtracting the static pressure from the total pressure, is plotted in Figure 10.

It can be clearly seen that the not only a vortex field in the wake of the ice ridge but also a vortex field at the internal wave peak occur in the two layer fluids. Each vortex field is a relatively low pressure zone with the lowest pressure at the vortex center, accounting for the reason why the fluid acts drag force on the ice ridge. In a single-layer flow, the drag force of the ice ridge is only affected by a low-pressure zone of the wake vortex. And as the velocity increases, the relative pressure of the center of the vortex decreases. However, in the two layers flow, the ice ridge drag is affected by both the wake vortex field after the ice ridge and the vortex field around the first internal wave peak.

Especially when the drag speed is less than the internal wave phase speed, the internal wave disturbance propagates simultaneously to the upstream and downstream of the ice ridge. Meanwhile, the internal wave is relatively stable with respect to the ice ridge, and moves following the movement of the ice ridge. The vortex field of the crest and the wake vortex field are coupled to each other to affect the drag force of the ice ridge.

As the speed increases, the internal wave peaks in Figure 10(c) move away from the ice ridge, and the influence of that field on the ice ridge is getting smaller and smaller, and the drag force gradually approaches that in the single layer flow. When $Fr$ = 0.71, the crest of the internal wave also reaches the highest point and the vortex region of the internal wave peak has the greatest influence on the wake vortex region. As Figure 10(b) shows, the wake vortex region is not sufficient, which seems to be squeezed between the internal wave crest and the ice ridge. The relative pressure of the wake vortex region is also the lowest value, so the drag force reaches an extreme value at this time.

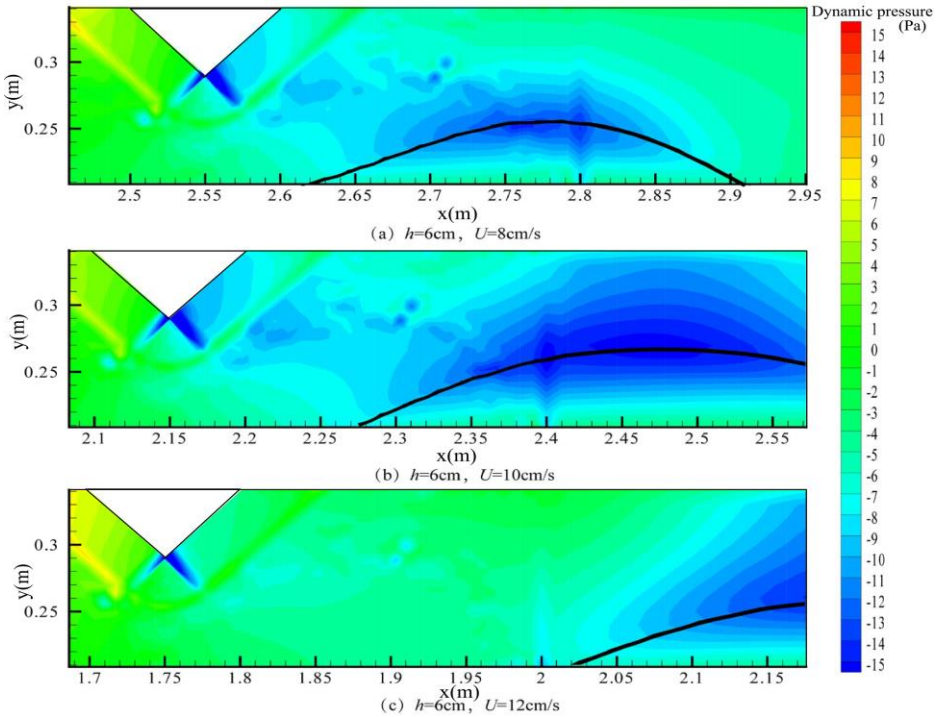


Figure 10. Instantaneous contours of dynamic pressure field in x-y plane when (a) $h$ = 6 cm, $U$ = 8 cm/s; (b) $h$ = 6 cm, $U$ = 10 cm/s; (b) $h$ = 6 cm, $U$ = 12 cm/s;

## CONCLUSIONS

The influence of factors on the drag force and coefficient of the ice ridge is discussed in this paper, including the Froude number and the ice ridge draught depth. The numerical simulation of the ice ridge drag force is basically consistent with the physical results.

When the keel depth of the ice ridge remains unchanged, the drag force increases first and then decreases with increasing *Fr* in the nonlinear part. The variation of the drag coefficient with Fr also has the nonlinear trend which is more obvious. When $Fr > 1$, the local drag coefficient of the ice ridge is stable at 1, similar with the results in uniform fluid.

When *Fr* remains constant, the drag coefficient of the ice ridge increases with the growth of the draught water depth. The gradient of the drag coefficient with dimensionless depth is relatively steep in the range of $Fr \leq 0.57$; When $Fr > 0.57$, the drag coefficient of the ice ridge does not change substantially with draught water depth, and finally close to 1.

In the transcritical region, the nonlinear law of the drag force with the variation of the Froude number is illustrated from two aspects, analyzing the interface displacement and the pressure field near the ice ridge. Moreover, the crest vortex region and the wake vortex region are coupled with each other. As the the displacement increases, the negative pressure region near the internal wave peak expands. And the negative pressure region in the wake of the ice ridge is also affected so that the interface displacement and the drag force are highly correlated. When the displacement reaches the maximum, the drag force reaches an extreme point. The internal wave shape produced by the numerical simulation agrees well with the internal wave shape in the physical tank. Due to the difference in the density distribution around interface, the physical simulation shows more mixing phenomenon and consumes more internal wave energy.

The local drag coefficient of a single ice ridge plays an important role in determining the ice-water drag coefficient. Combined with the shallow ocean stratification phenomenon often occurring in the Arctic summer sea ice marginal area, this paper preliminarily discusses the local drag coefficient under stratified fluid conditions. The local drag coefficient changes with the draught water depth of the ice ridge and the Froude number, which lays a foundation for the parameterization of the ice-water drag coefficient in the stratified fluid. In addition to the keel depth and the Froude number, changes of the ice ridge morphology and the stratified layer depth will also affect the local drag coefficient of the ice ridge. Further experimental research and theoretical analysis are needed to develop the parameterization of ice-water drag coefficient.

## REFERENCES


Amundrud, T. L., Melling, H., Ingram, R. G., & Allen, S. E., 2006. The effect of structural porosity on the ablation of sea ice ridges. *Journal of Geophysical Research: Oceans*, 111, C06004.

Andreas, E. L., 1995. Air-ice drag coefficients in the western Weddell Sea: 2. A model based on form drag and drifting snow. *Journal of Geophysical Research: Oceans*, 100(C3), 4833-4843.

Andreas, E. L., & Claffey, K. J., 1995. Air-ice drag coefficients in the western Weddell Sea: 1. Values deduced from profile measurements. *Journal of Geophysical Research: Oceans*, 100(C3), 4821-4831.

Baines, P. G., 1984. A unified description of two-layer flow over topography. *Journal of Fluid Mechanics*, 146, 127-167.

Fujisaki, A., Yamaguchi, H., Toyota, T., Futatsudera, A., & Miyanaga, M., 2009. Measurements of air-ice drag coefficient over the ice-covered Sea of Okhotsk. *Journal of oceanography*, 65(4), 487.

Grue, J., 2015. Nonlinear interfacial wave formation in three dimensions. *Journal of Fluid Mechanics*, 767, 735-762.

Han, H., Li, Z., Huang, W., Lu, P., & Lei, R., 2015. The uniaxial compressive strength of the Arctic summer sea ice. *Acta oceanologica sinica*, 34(1), 129-136.
Jameel, M. I., Rowe, R. D., & Topham, D. R., 1993. Stratified flow under an ice keel—a numerical approach. *International journal for numerical methods in fluids*, 16(5), 353-364.
Lu, P., Li, Z., & Han, H., 2016. Introduction of parameterized sea ice drag coefficients into ice free-drift modeling. *Acta Oceanologica Sinica*, 35(1), 53-59.
Lu, P., Li, Z., Cheng, B., & Leppäranta, M., 2011. A parameterization of the ice-ocean drag coefficient. *Journal of Geophysical Research: Oceans*, 116(C7).
Lüpkes, C., Gryanik, V. M., Hartmann, J., & Andreas, E. L., 2012. A parametrization, based on sea ice morphology, of the neutral atmospheric drag coefficients for weather prediction and climate models. *Journal of Geophysical Research: Atmospheres*, 117(D13).
McPhee, M. G., 2012. Advances in understanding ice–ocean stress during and since AIDJEX. *Cold Regions Science and Technology*, 76, 24-36.
Melville, W. K., & Helfrich, K. R., 1987. Transcritical two-layer flow over topography. *Journal of Fluid Mechanics*, 178, 31-52.
Mercier, M., Vasseur, R., & Dauxois, T., 2011. Resurrecting dead-water phenomenon. *arXiv preprint arXiv:*1103.*0903*.
Morison, J. H., McPhee, M. G., & Maykut, G. A., 1987. Boundary layer, upper ocean, and ice observations in the Greenland Sea marginal ice zone. *Journal of Geophysical Research: Oceans*, 92(C7), 6987-7011.
Mortikov, E. V., 2016. Numerical simulation of the motion of an ice keel in a stratified flow. *Izvestiya, Atmospheric and Oceanic Physics*, 52(1), 108-115.
Pease, C. H., Salo, S. A., & Overland, J. E., 1983. Drag measurements for first-year sea ice over a shallow sea. *Journal of Geophysical Research: Oceans*, 88(C5), 2853-2862.
Pite, H. D., Topham, D. R., & Van Hardenberg, B. J., 1995. Laboratory measurements of the drag force on a family of two-dimensional ice keel models in a two-layer flow. *Journal of Physical Oceanography*, 25(12), 3008-3031.
Randelhoff, A., Sundfjord, A., & Renner, A. H., 2014. Effects of a shallow pycnocline and surface meltwater on sea ice–ocean drag and turbulent heat flux. *Journal of Physical Oceanography*, 44(8), 2176-2190.
Snape, T. J., & Forster, P. M., 2014. Decline of Arctic sea ice: Evaluation and weighting of CMIP5 projections. *Journal of Geophysical Research: Atmospheres*, 119(2), 546-554.
Tan, B., Li, Z. J., Lu, P., Haas, C., & Nicolaus, M., 2012. Morphology of sea ice pressure ridges in the northwestern Weddell Sea in winter. *Journal of Geophysical Research: Oceans*, 117(C6).
Tsamados, M., Feltham, D. L., Schroeder, D., Flocco, D., Farrell, S. L., Kurtz, N., ... & Bacon, S., 2014. Impact of variable atmospheric and oceanic form drag on simulations of Arctic sea ice. *Journal of Physical Oceanography*, 44(5), 1329-1353.
White, B. L., & Helfrich, K. R., 2012. A general description of a gravity current front propagating in a two-layer stratified fluid. *Journal of Fluid Mechanics*, 711, 545-575.